Efficient Schiff Base Ligand for Selective Cd(II) and Pb(II) Removal from Water

Amal E. Mubark*[1], Sabreen M. El-Gamasy[2], Ahmed M. Masoud[1], **Adel A. El-Zahhar [3],** ***Majed M. Alghamdi [3], Mohamed H. Taha[1], Taha F. Hassanein[4]***

[1] Nuclear Materials Authority, P.O. Box 530, El Maddi, Cairo, Egypt
2Chemistry Department, Faculty of Science, Menoufia University, Shebin El-Koam, 00123 Egypt
[3]Department of Chemistry, Faculty of Science, King Khalid University, P.O.Box 9004, Abha 61413, Saudi Arabia
[4]Chemistry Department, Faculty of Science, Helwan University, 11795, Helwan, Cairo, Egypt

*Corresponding author: *amal_mubark2014@yahoo.com*

1. Sorbent characterization

The synthesized Schiff base ligand, 2-((E)-(4-aminophenylimino)methyl)benzoic acid, was characterized to evaluate its structural, morphological, and surface properties. X-ray diffraction (XRD) analysis, performed using a PANalytical X'PERT Pro diffractometer (Netherlands), assessed the crystallinity and phase composition. Fourier transform infrared spectroscopy (FTIR) confirmed the presence of key functional groups (-C=N, -COOH, $-NH_2$) essential for metal adsorption, using a PerkinElmer Spectrum One spectrometer (USA). The surface morphology and elemental composition were examined using scanning electron microscopy (SEM) and energy-dispersive X-ray spectroscopy (EDX) with a JEOL-JSM 6360 microscope (Japan). Thermal stability and decomposition behavior were investigated through thermogravimetric analysis (TGA) using a TGA Q50 analyzer (TA Instruments, USA) under a nitrogen atmosphere. N_2 adsorption-desorption isotherms, analyzed using the BET and BJH methods, determined surface area and pore structure with a NOVA 3200 apparatus (USA). The zeta potential and particle size distribution, measured via a Zetasizer Nano ZS (UK), provided insights into colloidal stability and hydrodynamic diameter. The ligand's molecular structure was further confirmed through ^{1}H-NMR spectroscopy using a Bruker Avance III 400 MHz spectrometer (Germany) with DMSO-d_6 as the solvent. Finally, mass spectrometry (MS) verified molecular weight and purity using a Q-TOF mass spectrometer (USA).

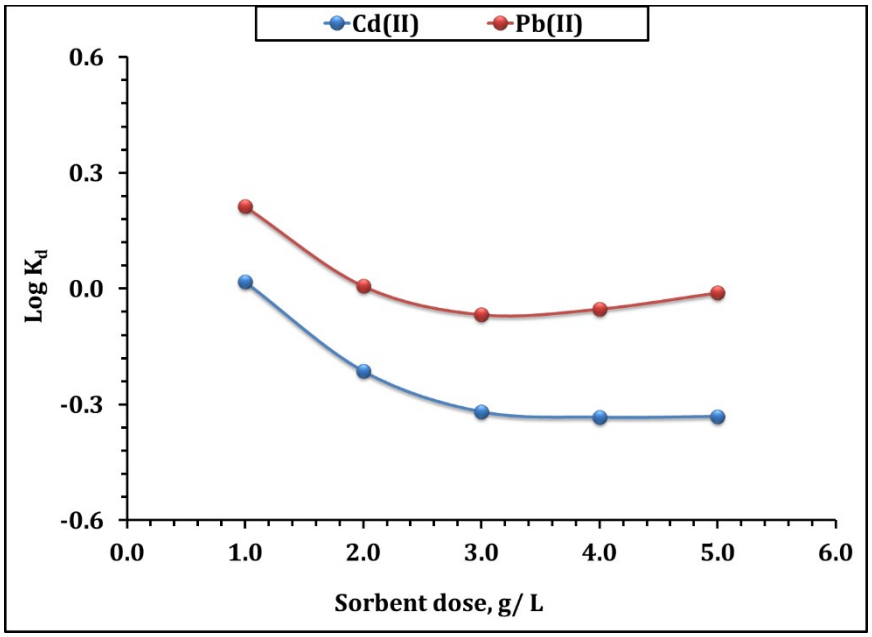

Figure S1: *Effect of ligand dose on distribution coefficient (logKd) for Cd(II) and Pb(II) from synthetic aqueous solutions (pH 5.9; time of 240 min; original concentration: 100 mg/ L; and room temperature).*

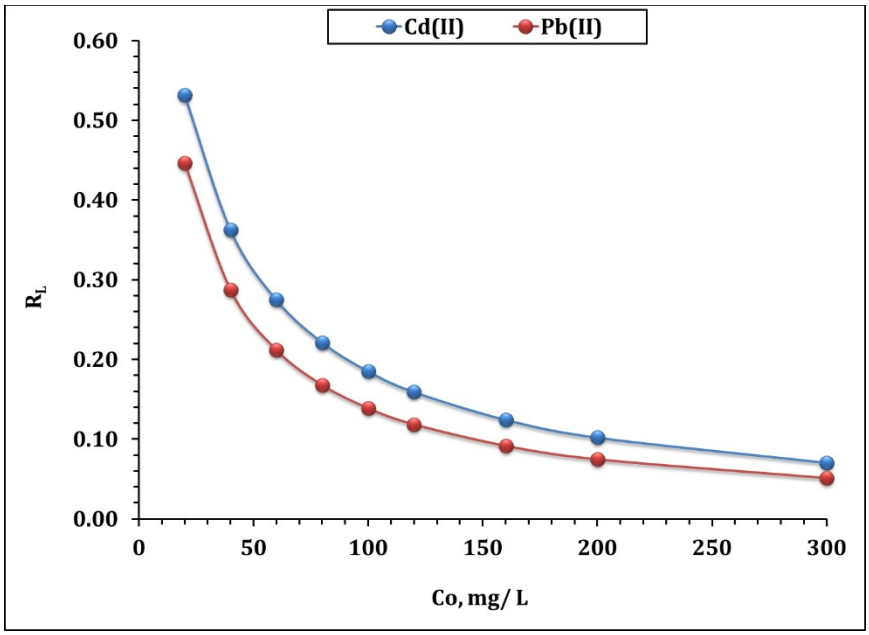

Figure S2: *Separation factor (R_l) for Cd(II) and Pb(II) adsorption from synthetic aqueous solutions across various initial concentrations.*

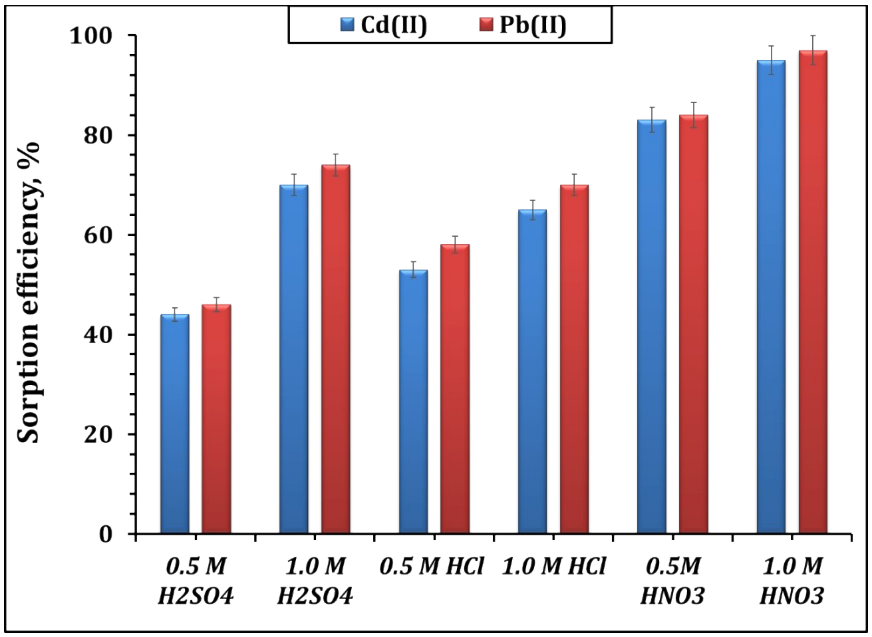

Figure S3: *Desorption efficiency of Cd(II) and Pb(II) from loaded ligand using different eluents (shaking: 240 min; room temperature; and ligand dosage: 1.0 g/ L).*

Table S1: *Kinetic, isotherm, and thermodynamics equations for Cd(II), and Pb(II) adsorption process* ***[1-9]***.

Kinetics	Equations
Pseudo-first-order	$q_t = q_1\left(1 - e^{-k1t}\right)$
Pseudo-second-order	$q_t = \dfrac{1}{\left(1 \middle\vert k_2 q_2^2\right) + \left(t \middle\vert q_2\right)}$
Intra-particle diffusion model (IPD)	$q_t = K_{id}\, t^{0.5} + C_i$
Isotherms	**Equations**
Langmuir model	$q_e = \dfrac{q_m k_L C_e}{1 + k_L C_e}$
Freundlich model	$q_e = K_F C_e^{1/n_F}$
Temkin model	$q_e = \dfrac{RT}{b_T} \ln K_T C_e$
Sips model	$q_e = \dfrac{q_S \left(k_S C_e\right)^{mS}}{1 + \left(k_S C_e\right)^{mS}}$
Thermodynamics	**Equations**
	$\log K_C = -\dfrac{\Delta H^o}{2.303\, R} X \dfrac{1}{T} + C$ $-\Delta G^o = 2.303\, RT \log K_C$ $\Delta G^o = \Delta H^o - T\, \Delta S^o$
Fitting	**Equations**
Coordination coefficient (R^2)	$R^2 = 1 - \dfrac{\sum_1^n \left(q_{exp} - q_{pred}\right)^2}{\sum_1^n \left(q_{exp} - \bar{q}_{exp}\right)^2}$

Average relative error (ARE)	$ARE = \frac{100}{n}\sum_{1}^{n}\frac{\lvert q_{exp} - q_{pred}\rvert}{q_{exp}}$

qe (mg g^{-1}) is the equilibrium concentration of Cd(II) species, and qt (mg g^{-1}) is the adsorbed amount of Cd(II) species ions after time t (min), Ce (mg L^{-1}) is equilibrium concentration of Cd(II) species. k_1 (min^{-1}) and k_2 (min^{-1}) are the rate constants for the pseudo first and second order, respectively. K_{id} (mg/g. $min^{0.5}$) is a rate constant, and C is the thickness of the boundary layer. q_m and q_S are the maximum sorption capacity (mg. g^{-1}) of Langmuir and Sips models. k_L (L. mg^{-1}), K_F (L/ mg), K_T (L min^{-1}), and K_S (L/ mg) are represent the constants of Langmuir, Freundlich, Temkin, and Sips models. n refer to the sorption intensity, b_T is Temkin constant that refers to the adsorption heat, mS is Sips constant. $\boldsymbol{q_s}$ is the theoretical isotherm saturation capacity (mg/g). K_C is a non-dimensional equilibrium constant and it equals K_d X 1000 X ρ **[4-5]**; T is the temperature (K), $\boldsymbol{R}$ is the universal gas constant (8.314 J mol^{-1}. K^{-1}), ρ is solution density g/ L, and C is a constant. R^2 and x^2 are the coordination and Chi-square coefficients respectively, the number of test points is n, the experimental equilibrium capacity is q_{exp} (mg g^{-1}), while the predicted capacity is q_{pred} (mg g^{-1}).

References:

1) Hu, Q., Pang, S. and Wang, D., 2022. In-depth insights into mathematical characteristics, selection criteria and common mistakes of adsorption kinetic models: A critical review. *Separation & Purification Reviews*, *51*(3), pp.281-299.

2) González-López, M.E., Laureano-Anzaldo, C.M., Pérez-Fonseca, A.A., Arellano, M. and Robledo-Ortíz, J.R., 2022. A critical overview of adsorption models linearization: methodological and statistical inconsistencies. *Separation & Purification Reviews*, *51*(3), pp.358-372.

3) Tho, P.T., Van, H.T., Nguyen, L.H., Hoang, T.K., Tran, T.N.H., Nguyen, T.T., Nguyen, T.B.H., Le Sy, H., Tran, Q.B., Sadeghzadeh, S.M. and Asadpour, R., 2021. Enhanced simultaneous adsorption of As (iii), Cd (ii), Pb (ii) and Cr (vi) ions from aqueous solution using cassava root husk-derived biochar loaded with ZnO nanoparticles. *RSC advances*, *11*(31), pp.18881-18897.

4) Sharma, R., Sarswat, A., Pittman, C.U. and Mohan, D., 2017. Cadmium and lead remediation using magnetic and non-magnetic sustainable biosorbents derived from Bauhinia purpurea pods. *RSC advances*, *7*(14), pp.8606-8624.

5) Chen, X., Hossain, M.F., Duan, C., Lu, J., Tsang, Y.F., Islam, M.S. and Zhou, Y., 2022. Isotherm models for adsorption of heavy metals from water-a review. *Chemosphere*, *307*, p.135545.

6) Majd, M.M., Kordzadeh-Kermani, V., Ghalandari, V., Askari, A. and Sillanpää, M., 2022. Adsorption isotherm models: A comprehensive and systematic review (2010−2020). *Science of The Total Environment*, *812*, p.151334.

7) Taha, M.H., 2021. Sorption of U (VI), Mn (II), Cu (II), Zn (II), and Cd (II) from multi-component phosphoric acid solutions using MARATHON C resin. Environmental Science and Pollution Research, 28(10), pp.12475-12489.

8) Ebelegi, A.N., Ayawei, N. and Wankasi, D., 2020. Interpretation of adsorption thermodynamics and kinetics. *Open Journal of Physical Chemistry*, *10*(3), pp.166-182.

Table S2: *The values of Morris-Weber model parameters.*

		Cd(II)	**Pb(II)**
Weber and Morris model	**k_i (mg/g min$^{1/2}$)**	1.68	2.23
	C	14.2	12.0
	R^2	0.96	0.96

Table S3: *Sorption capacity (mg/ g), and desorption efficiency (%) for Cd(II) and Pb(II) recovery for five successive cycles.*

	Cd(II)		**Pb(II)**	
Cycle	Adsorption Capacity (mg/g)	Desorption Efficiency (%)	Adsorption Capacity (mg/g)	Desorption Efficiency (%)
1	51.9	95.1	62.1	97.1
2	51.2	94.3	61.5	95.8
3	50.4	92.8	60.2	93.2
4	48.8	89.2	58.4	89.9
5	47.5	86.1	56.7	86.9

Table S4: *The chemical analysis of the real waste raffinate solution before and after the adsorption process.*

Element	Concentration, mg/ L		E, %
	Initial	Final	
Pb	92	35	62.0
Cd	88	43	51.1
Cr	70	54	22.9
Y	85	65	23.5
Si	230	197	14.3
Cl-	600	580	3.3
K	690	675	2.2
Na	280	250	10.7